

Mesh Denoising based on Normal Voting Tensor and Binary Optimization

S.K. Yadav, U. Reitebuch, and K. Polthier

Abstract—This paper presents a tensor multiplication based smoothing algorithm that follows a two step denoising method. Unlike other traditional averaging approaches, our approach uses an element based normal voting tensor to compute smooth surfaces. By introducing a binary optimization on the proposed tensor together with a local binary neighborhood concept, our algorithm better retains sharp features and produces smoother umbilical regions than previous approaches. On top of that, we provide a stochastic analysis on the different kinds of noise based on the average edge length. The quantitative and visual results demonstrate the performance our method is better compared to state of the art smoothing approaches.

Index Terms—Geometry Processing, Mesh Smoothing, Normal Voting Tensor, Eigenvalue Binary Optimization, Noise Analysis.



1 INTRODUCTION

MESH denoising is a central preprocessing tool in discrete geometry processing with many applications in computer graphics such as CAD, reverse engineering, virtual reality and medical diagnosis. The acquisition of 3D surface data takes place using the 3D measurement technologies such as 3D cameras and laser scanners. During the surface measurement, noise is inevitable due to various internal and external factors which degrades surface data quality and its usability. The main goal of any mesh denoising algorithm is to remove spurious noise and compute a high quality smooth function on the triangle mesh while preserving sharp features.

In general, noise and sharp features both have high frequency components, so decoupling the sharp features from noise is still a challenging problem in mesh denoising algorithms. Traditionally, noise is removed by using a low pass filtering approach, but this operation leads to feature blurring. A variety of Laplacian based surface smoothing algorithms are available to overcome the problem of feature blurring. Our smoothing approach uses the eigenanalysis and a binary optimization of the proposed element based normal voting tensor to decouple noise and sharp features. We design an iterative denoising method that removes low and high frequent noise while preserving sharp features in smooth surfaces. Our algorithm does not produce piecewise flat areas, i.e. false features in the denoised triangular mesh.

1.1 Contributions

We introduce a simple and effective mesh denoising algorithm which does not follow the classic Laplacian approach of surface smoothing. Our algorithm follows a two stage de-noising process. In the first stage, we process noisy face normals. In the second stage, we update the vertex positions accordingly. Our contributions are as follow:

- We propose a tensor multiplication based smoothing technique with proper convergence property to remove the undesired noise from noisy surfaces.
- We apply a binary optimization technique on the eigenvalues of the propose element based normal voting tensor that helps us to retain sharp features in the concerned geometry and improves the convergence rate of the algorithm.
- We give a stochastic analysis of the effect of noise on the triangular mesh based on the average edge length of the elements in the geometry. It gives an upper bound to the noise standard deviation to have minimum probability for flipped element normals.

2 RELATED WORK

In the last two decades, a wide variety of smoothing algorithms has been introduced to remove undesired noise while preserving sharp features in the geometry. The most common technique for noise reduction is mainly based on the Laplacian on surfaces. We can characterize them as isotropic, anisotropic and two stage smoothing methods. For a comprehensive review on mesh denoising, we refer to [1] and [2]. We mention a major part of related works in this section.

Isotropic smoothing methods are the earliest smoothing algorithms. These algorithms have low complexity but suffer from severe shrinkage and further feature blurring [3]. Desbrun et al. [4] introduced an implicit smoothing algorithm that produces stable results against irregular meshes and avoids the shrinkage by volume preservation. Later, the concept of the differential coordinates is introduced by Alexa [5] as a local shape descriptor of a geometry. Su et. al. exploited the differential coordinates concept for mesh denoising by computing the mean of the differential coordinates at each vertex and then compute a smooth surface according to the mean differential coordinates [6]. This method produces less shrinkage but is unable to preserve shallow features. The differential coordinates framework is extended for a variety of mesh processing algorithms by [7]. In general, isotropic

• S. K. Yadav, U. Reitebuch and K. Polthier are with the Department of Mathematics and Computer Science, Freie Universitaet, Berlin.
E-mail: sunil.yadav@fu-berlin.de

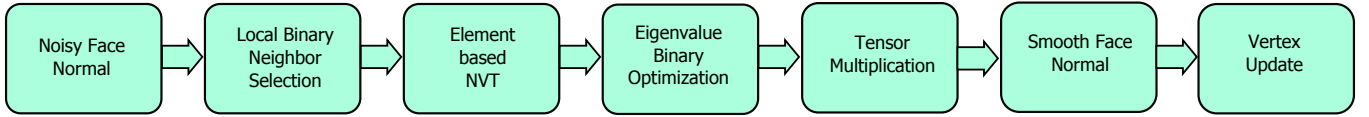


Figure 1: The pipeline for the proposed smoothing algorithm.

smoothing methods are prone to shrink volumes and blur features but effective in noise removal.

Anisotropic diffusion is a PDE based de-noising algorithm introduced by Perona and Malik [8]. The same concept was extended for surface denoising using a diffusion tensor [9] [10]. Similarly, the anisotropic diffusion of surface normals was introduced for surface smoothing [11]. Later, the prescribed mean curvature based surface evolution algorithm was introduced by [12] that avoids the volume shrinkage and preserves features effectively during the denoising process. Several other algorithms related to anisotropic diffusion are based on the bilateral smoothing [13] which was initially introduced by Tomasi et. al. [14] for image smoothing. Researchers have proposed a general framework for bilateral and mean shift filtering in any arbitrary domain [15]. These algorithms are simple and effective against noise and feature blurring. In general, anisotropic denoising methods are more robust against volume shrinkage and are better in terms of feature preservation but the algorithm complexity is higher compared to the isotropic algorithms.

The two step denoising methods are simple and quite robust against noise. These algorithms consist of two steps: face normal smoothing and vertex position update. Face normals are treated as signals on the dual graph of the mesh with values in the unit sphere. The Laplacian smoothing of the face normals on the sphere is introduced by [16] where displacement of the concerned face normal is computed along a geodesic on the unit sphere. The face normal smoothing is done by rotating the face normal on the unit sphere according to the weighted average of the neighbor face normals. Different linear and non-linear weighting functions have been introduced by different algorithms for face normal smoothing. For example, Yogou et.al. [17] computed the mean and the median filtering of face normals to remove noise effect. Later, a modified Gaussian weighting function was applied to face normal smoothing in an adaptive manner to reduce the feature blurring [18]. In continuation, the alpha trimming method introduced a non-linear weighting factor which approximates both, the mean and the median filtering [19]. Bilateral normal is one of most effective and simple algorithms among the two step methods [20] where the weighting function is computed based on the normal differences (similarity measurement) and spatial distances between neighboring faces. Recently, a total variational method has been also introduced for mesh normal filtering [21]. After the preprocessing of the face normals, vertex position update is done by using the orthogonality between the corresponding edge vector and the face normal [22]. The two step denoising methods are simple in implementation and produce effective results. However, on noisy surfaces, it is difficult to compute the similarity

function because of the ambiguity between noise and sharp features, and which leads to unsatisfactory results.

In recent mesh denoising methods, the compressed sensing techniques are involved to preserve sharp features precisely and remove noise effectively [23]. For example, the L_0 mesh denoising method assumed that features are sparse on general surfaces and introduced an area based differential operator. This method utilizes the L_0 optimization to maximize the flat region on noisy surfaces to remove noise [24]. The L_0 method is effective against the high noise but also produces piecewise flat area on smooth surfaces. Later, the weighted L_1 -analysis compressed sensing optimization is applied to recover sharp features from the residual data after global Laplacian smoothing [25]. Recently, the ROF (Rudin, Osher and Fatemi) based algorithm has been introduced in [26]. This method applies L_1 optimization on both data fidelity and regularization to remove noise without volume shrinkage. In general, the compressed sensing based denoising algorithms are robust against high intensity noise and recover not only the sharp features but also the shallow features, but at the same time these algorithms produce false features (piecewise flat areas) on smooth geometries.

A multistage denoising framework was introduced by [27] [28] where feature identification is done by the eigenanalysis of the NVT(normal voting tensor) [29] [30] and then the whole geometry is divided into different clusters based on the features and the smoothing is applied on different clusters independently. Later, the guided mesh normals are computed based on the consistence normal orientation and bilateral filtering is applied [31]. Recently, Wei et. al. [32] exploited both vertex and face normal information for feature classification and surface smoothing. In continuation, researchers detect features on the noisy surface using quadratic optimization and then remove noise using L_1 optimization while preserving features [33]. Multistage denoising algorithms produce effective results against different levels of noise but have higher algorithm complexity because of the different stages.

Our method follows a two step denoising algorithm where the face normal smoothing is motivated by the NVT based algorithms. In the proposed method, noise and features are decoupled using the eigenanalysis of the proposed element based normal voting tensor and noise is removed by the proposed tensor multiplication.

3 ALGORITHM OVERVIEW

Figure 1 shows the whole pipeline of our algorithm. The face normal smoothing consists of four steps: 1). We compute the geometric neighborhood for the concerned face using a local binary scheme. 2). We define the element based normal voting tensor within its geometric neighborhood. 3). To remove noise effectively, we apply a binary optimization

on the eigenvalues of the computed tensor. 4). We multiply the modified tensor to the corresponding face normal to suppress the noise. In the last stage, we update the vertex positions using the orthogonality between the edge vectors and the face normals.

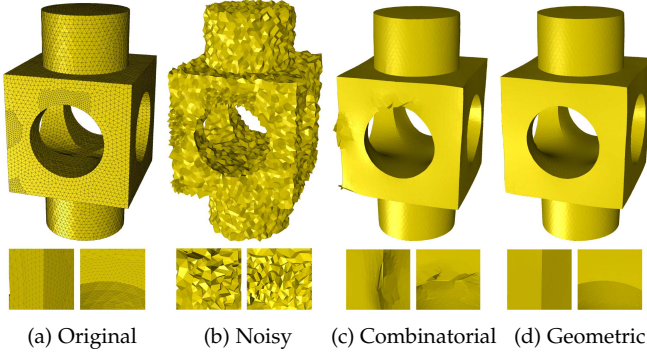


Figure 2: Comparison between geometric and combinatorial neighborhood on a non-uniform mesh block model. Figure(c) and (d) shows the results obtained by our method using the combinatorial and geometric neighborhood.

4 METHOD

In this section, we explain each stage of the proposed algorithm briefly. We follow the method development procedure as shown in figure 1.

4.1 Local Binary Neighbor Selection

The first step of our de-noising scheme is the preprocessing of the face normals using the neighboring face normals. To select the neighborhood area Ω , there are three possibilities: Topological, geodesic and geometrical neighborhood. The geometrical neighborhood depends only on the radius of the disk irrespective of mesh resolution unlike the topological neighborhood. Figure 2 shows that the geometrical neighborhood is more effective against irregular meshes compared to the topological neighborhood. Geodesic neighborhood is quite similar to the geometrical neighborhood but it is not appropriate when a model is corrupted by high intensity of noise. We apply these neighborhood concepts along with a local binary neighbor selection.

The idea of a local binary neighbor selection is inspired from the local binary pattern in image processing, mainly used for feature description [34]. The local binary pattern assigns ones to the neighborhood pixels if surrounding pixel values are greater than the central pixel and zeros otherwise. Similarly, we select neighbor elements based on a threshold value ρ . Based on the angle threshold, we assign a binary value to the neighborhood elements f_j w.r.t. central element f_i using the following function:

$$w_{ij} = \begin{cases} 1 & \text{if } \angle(\mathbf{n}_i, \mathbf{n}_j) \leq \rho \\ 0.1 & \text{if } \angle(\mathbf{n}_i, \mathbf{n}_j) > \rho \end{cases} \quad (1)$$

Where \mathbf{n}_i and \mathbf{n}_j are the face normals of the central element and the neighbor elements. By the value of 0.1, close to a feature, we still allow the area on the other side of the

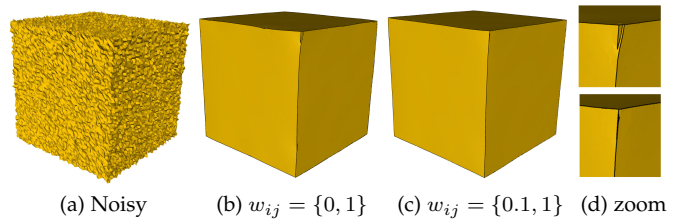


Figure 3: The results obtained by the proposed algorithm using the weight function mentioned in equation 1 and replacing the value 0.1 to 0 ($w_{ij} = \{0, 1\}$). The figure (d) shows that the weight function mentioned in equation 1 is more effective compared to the exact binary weighting ($w_{ij} = \{0, 1\}$).

feature to contribute (so the edge direction can be detected from the computed tensor), but the area on the "same" side of the feature will be dominant. Figure 3 shows that the contribution of the other side of the feature helps to enhance the sharp corner (figure 3-d). Our proposed weighting function is a discontinuous box filter which takes similar faces into consideration and avoids blurring features within the user defined geometric neighborhood. We are not using a distance based weighting function like bilateral filter. The proposed weighting function depends on the dihedral angle, which can be unstable initially but with iteration it becomes stable as shown in figure 4.

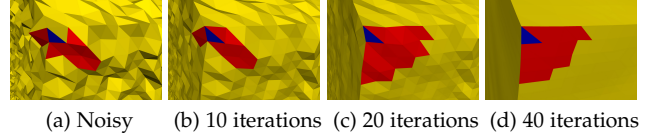


Figure 4: Figure shows the local binary neighbor selection in the proposed algorithm. Initially, it selects very few neighbor elements f_j (red color) around the central element f_i (blue) because of the dihedral angle threshold. As iterations increase, it selects more elements with similar element normals.

4.2 Element Based Normal Voting Tensor

Face normals give better a description about sharp features than vertex normals because the angle between the face normals are bigger compared to the angle between vertex normals in those regions.

We define an element based normal voting tensor on every element of a properly oriented triangulated mesh similar to the vertex based voting tensor proposed in [29]. The element based normal voting tensor is the weighted average of the covariance matrices of the geometrical or the topological neighbor elements. On the face f_i , it is defined as:

$$C_i = \frac{1}{\sum_{j \in \Omega} w_{ij}} \sum_{j \in \Omega} w_{ij} A_j \mathbf{n}_j \cdot \mathbf{n}_j^T \quad (2)$$

Where A_j is the area of the corresponding neighbor element f_j and w_{ij} is the weighting function as mentioned in the

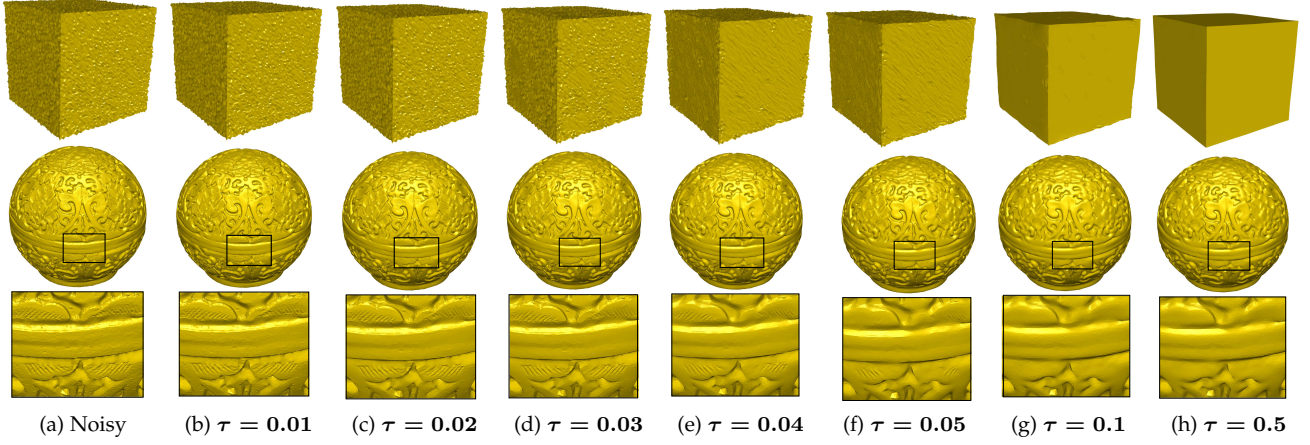


Figure 5: The figure shows the effect of the eigenvalue binary optimization threshold value τ on results of the proposed algorithm. The first row shows the cube model ($|V| = 24578$, $|F| = 49152$) corrupted by synthetic Gaussian noise ($\sigma_n = 0.4l_e$) and the second row shows the scanned box model (**real data** with $|V| = 149992$, $|F| = 299980$) and corresponding results regarding different value of τ . The third row shows the magnified area of the box model. For the box model, the algorithm produced the optimal result with smaller value of $\tau = 0.03$ because of low noise whereas the cube model needed the higher value of $\tau = 0.5$ because of high intensity noise. The bigger value of the τ can lead to the feature blurring as shown in figure (h) for the box model.

equation 1. Weighting by corresponding element area makes the proposed tensor more robust against irregular sampling. We can define the proposed tensor in \mathbb{R}^3 space without the C^2 restriction of surfaces. The eigenanalysis of the given tensor identifies features on triangulated surfaces similar to the methods [29] and [28]. In our algorithm, the proposed tensor is represented as a mesh denoising operator which is able to suppress the noise contents from noisy surfaces while preserving sharp features. The similarity between the proposed tensor and the shape operator is discussed in the appendix. The element based normal voting tensor $C_i : \mathbb{R}^3 \rightarrow \mathbb{R}$ is a symmetric and positive semi definite matrix so we can represent C_i using an orthonormal basis of the eigenvectors e_k and real eigenvalues λ_k :

$$C_i = \sum_{k=0}^2 \lambda_k e_k e_k^T \quad (3)$$

Geometrical Interpretation: On a noise free triangulated mesh, a planar area has only one dominant eigenvalue in surface normal direction. Two dominant eigenvalues indicate edge features where the weakest eigenvector will be along the edge direction. At a corner all three eigenvalues are dominant. Consider a cube model where the eigenvalue vector is sorted and normalized, then for orthogonal features we can write: $\{\lambda_1 = 1, \lambda_2 = \lambda_3 = 0\}$ (face), $\{\lambda_1 = \lambda_2 = \frac{\sqrt{2}}{2}, \lambda_3 = 0\}$ (edge) and $\{\lambda_1 = \lambda_2 = \lambda_3 = \frac{\sqrt{3}}{3}\}$ (corner).

4.3 Eigenvalues Binary Optimization

Let us consider a noisy mesh, corrupted by a random noise with standard deviation σ_n bounded by average edge length and eigenvalues of the element based normal voting tensor are sorted in decreasing order ($\lambda_1 \geq \lambda_2 \geq \lambda_3 \geq 0$). On a planar area (face) of the geometry: $\lambda_1 \gg \sigma_n$, and $\lambda_2, \lambda_3 \propto \sigma_n$. Similarly, on an edge of the geometry: $\lambda_1, \lambda_2 \gg \sigma_n$ and

$\lambda_3 \propto \sigma_n$. On a corner of the geometry: $\lambda_1, \lambda_2, \lambda_3 \gg \sigma_n$. We apply binary optimization to remove noise effectively

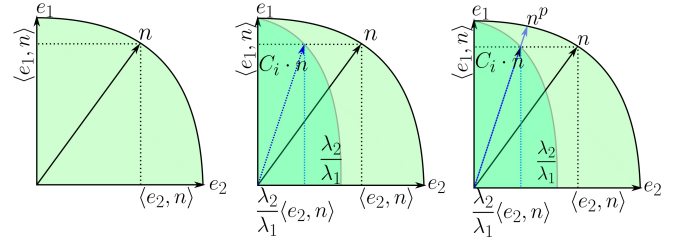


Figure 6: The figure shows the basic idea behind the proposed method to remove noise in \mathbb{R}^2 where e_i and λ_i represent the eigenvectors and eigenvalues of the proposed element based voting tensor and n shows the noisy normal. We project the noisy normal n towards the dominant eigendirection e_1 by corresponding tensor multiplication.

by setting the less dominant eigenvalues to zero and the dominant eigenvalues to one. Our optimization technique removes noise not only from the planar area but also along the edge direction of sharp features during the denoising process. We implemented the binary optimization by introducing a scalar threshold value τ . The less dominant eigenvalues depend on noise intensity so the threshold value should be $\tau \propto \sigma_n$. The threshold value τ has been chosen such that dominant eigenvalues will be bigger than the threshold value τ . We modify the eigenvalues of the computed tensor using the eigenvalues binary optimization. The λ are modified eigenvalues due to the binary optimization. There are three eigenvalues for feature classification so our optimization method checks following three cases:

- At a corner of noisy surfaces (smooth or sharp), the minimum of eigenvalues should be bigger than the

threshold value i.e. $\lambda_3 \geq \tau$, Hence :

$$\tilde{\lambda}_i = 1, \quad i = \{1, 2, 3\} \quad \text{if } \lambda_3 \geq \tau$$

- At an edge of noisy geometry (smooth or sharp), the less dominant eigenvalue should be smaller than the threshold value i.e. $\lambda_3 \leq \tau$ and $\lambda_2 \geq \tau$, hence:

$$\tilde{\lambda}_2 = \tilde{\lambda}_1 = 1, \quad \tilde{\lambda}_3 = 0 \quad \text{if } \lambda_2 \geq \tau, \quad \lambda_3 \leq \tau$$

- In the last case, we check for the planar area of the geometry. Having $\lambda_2 \leq \tau$ and $\lambda_3 \leq \tau$ show that the only dominant eigenvalue is λ_1 , hence :

$$\tilde{\lambda}_1 = 1, \quad \tilde{\lambda}_2 = \tilde{\lambda}_3 = 0 \quad \text{if } \lambda_1 \geq \tau, \quad \lambda_3, \lambda_2 \leq \tau$$

These three are the possible combinations during the eigenvalue binary optimization. The threshold τ can be set by the user according to the noise intensity.

Remark: In curved regions of the geometry, we get one dominant eigenvalue for the normal direction and two weak eigenvalues for the tangential directions - usually the eigenvectors will align with curvature directions. All curved areas, where no sharp edge or corner is detected, are treated as locally planar areas. To see the effect of different values of τ , we have experimented with two different models, the Box model (real data, with different level of features and less noise) and the Cube model (with limited features and high noise). With smaller values of $\tau = 0.01 - 0.05$, there is not much change on the cube model because of the higher noise whereas the box model manages to removes the noise and also the shallow features with increasing τ . So τ is responsible for the removing noise and also for preserving features. If the feature size is smaller than the noise intensity, it would be really difficult to preserve.

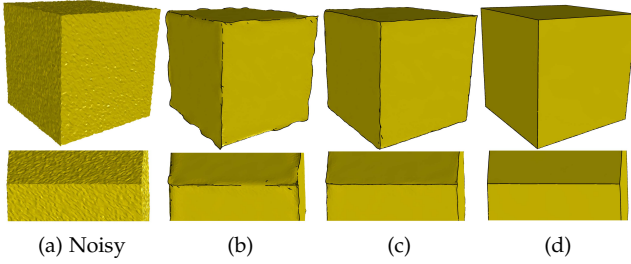


Figure 7: From left to right: (a): Noisy cube model, (b): The result without using the eigenvalues binary optimization and local binary neighborhood selection. (c): The result without the local binary neighbor selection. (d): The result obtained by using both eigenvalues binary optimization and local binary neighborhood selection. Sharp edges are drawn by black lines.

4.4 De-Noising via Tensor Multiplication

Idea: Traditionally, the face normal smoothing is done by rotating the concerned face normal along a geodesics on the unit sphere whereas our method aligns the face normals by the projection. We project noisy face normals towards the smooth normals by tensor multiplication. Our tensor multiplication method is inspired from the feature classification characteristic of the eigenvalues. If the noise standard

deviation is bounded by the average length in geometry mentioned in section 4.5, then the value of the smallest eigenvalue and differences between two eigenvalues is not significant. In the eigen analysis of the tensor, the weakest eigen direction (smallest eigenvalue) represents noise (not at the corner). Multiplication of the average covariance matrix to the corresponding element normal will suppress the noise in the weak eigendirection. This operation also strengthens the element normal in the strongest eigendirection. A demonstration of the tensor multiplication to the corresponding noisy face normal is shown in figure 6 in \mathbb{R}^2 . If $\lambda_2 > \lambda_1$, then it will strengthen the face normal in the desired direction \mathbf{e}_1 and suppressed noise in the \mathbf{e}_2 direction. We can mention the whole procedure in following steps:

- Noisy face normal \mathbf{n} is decomposed on the eigenbasis (\mathbf{e}_1 and \mathbf{e}_2) of the element based normal voting tensor, figure 6 (left).
- Then the modified eigenvalues (λ_1 and λ_2) get multiplied in the corresponding eigendirections to suppress the weak eigenvalue in weak eigendirection, figure 6 (middle).
- Finally the new normalized element normal \mathbf{n}^p , in figure 6 (right).

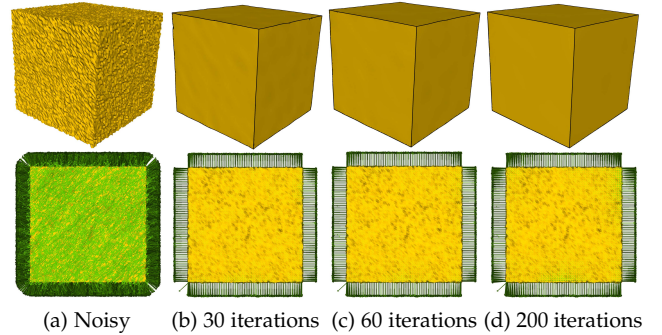


Figure 8: Stable convergence: The first row shows results with different number of iterations and second row show the corresponding processed face normals (XY-plane view). (a): Noisy cube model, (b): The result after 30 iteration (c): The result after 60 iteration. (d): The result after 200 iteration. There is no significant between the figure (b) and (c).

4.4.1 Anisotropic Face Normal Denoising

We can recompute the element based normal voting tensor by using the same eigenvectors with modified eigenvalues.

$$\tilde{C}_i = \sum_{k=0}^2 \tilde{\lambda}_k \mathbf{e}_k \mathbf{e}_k^T$$

\tilde{C}_i will have the quantized eigenvalues according to the different features on the surface. To apply this effect on noisy surfaces, we multiply the corresponding element normal with the newly computed tensor \tilde{C}_i . The multiplication will lead to noise removal while retaining sharp features.

$$\tilde{\mathbf{n}}_i = \tilde{C}_f \mathbf{n}_i = \sum_{k=0}^2 \tilde{\lambda}_k \langle \mathbf{e}_k, \mathbf{n}_i \rangle \mathbf{e}_k$$

We can compute smooth face normals iteratively.

$$\tilde{\mathbf{n}}_i^{p+1} = \text{Normalize}(d\mathbf{n}_i^p + \tilde{C}_f^p \mathbf{n}_i^p) \quad (4)$$

Where p denotes the number of iteration and d is the damping factor to control the speed of preprocessing of the face normals. We use $d = 3$ for all experimentation.

4.4.2 Vertex Update

In the second stage of the denoising algorithm, we synchronize the vertex position with corresponding newly computed face normals. To compute the proper vertex position, the orthogonality between edge vectors and face normals is used [16] [22]. An energy function is then defined as follows.

$$\min_v \sum_{j \in N_v(i)} \sum_{(i,j) \in \partial F_k} \|\tilde{\mathbf{n}}_k \cdot (v_i - v_j)\|^2 \quad (5)$$

Where v_i is the vertex position and N_v represents the vertices count of the vertex star of v_i . ∂F_k is the boundary edge of the vertex star of v_i shared with face f_k . $\tilde{\mathbf{n}}_k$ is the smooth face normal at f_k . Taubin [16] explained that the face normal vector can be decomposed in to normal and tangential component and the main problem here is to find the vertex positions which minimize the tangential error. The possible solution of equation 5 may be a mesh with degenerate triangular faces. Like Taubin [16], to avoid the degenerate solution, we are using gradient descent that will lead to the optimal vertex positions.

$$\tilde{v}_i^{p+1} = v_i^p + \frac{1}{F(v_i)} \sum_{j \in N_v(i)} \sum_{(i,j) \in \partial F_k} \tilde{\mathbf{n}}_k \cdot (v_i - v_j) \quad (6)$$

Where $F(v_i)$ is the number of face connected to the vertex v_i and p denotes number of iterations. The iterative scheme also allows user to control the amount of smoothing.

4.5 Noise Analysis

Noise is inevitable during digital data acquisition of real life object using different devices. Modelling of the noise characteristics on the 3D triangulated mesh is a challenging problem. There are very few state of art reports available related to the noise analysis on triangulated 3D surface [36]. We give an analysis of the relation between noise and geometry resolution. Let us consider a smooth triangular mesh \mathcal{M}_s which is corrupted by a noise \mathcal{N} , $\mathcal{M} = \mathcal{M}_s + \mathcal{N}$. Where \mathcal{N} is noise caused by a scanning device and data acquisition process. Noise \mathcal{N} can be approximated by a random vector X_n consisting of three independent random variables. The random vector X_n follows the Gaussian distribution. Lets consider σ_n is the standard deviation of noise in each independent direction, then: $\{P\{|X_n| \leq \sigma_n\} = 0.682, P\{|X_n| \leq 2\sigma_n\} = 0.954, P\{|X_n| \leq 3\sigma_n\} = 0.997\}$.

Let us consider an edge vector l defined by using two vertices v_0 and v_1 in \mathbb{R}^2 : $l = (v_0 - v_1)$ if there is no noise, $l' = (v_0' - v_1')$ if noise is present. We give a probabilistic estimation of the effect of noise on the edge l w.r.t. the noise intensity (standard deviation) σ_n . Our analysis is mainly focused on the proper orientation of the edge normals. Wrong orientation of the edge normal \mathbf{n}_l leads to an edge flip in the smooth geometry as shown in figure 16. We

denote by Ω_1 and Ω_2 the sets of correctly oriented edge normal and wrong oriented edge normal respectively. The probabilistic estimation of the orientation of the edge normals based noise intensity and edge length is given as follow.

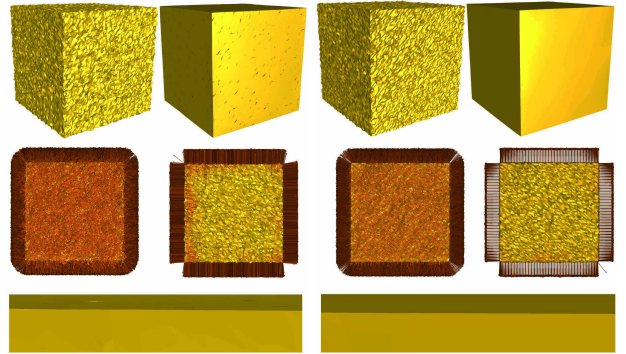
- Probability of an edge to have a correctly oriented edge normal:

$$P\{\tilde{\mathbf{n}}_l \in \Omega_1\} = \begin{cases} 0.682 & \text{if } \sigma_n \leq \frac{|l|}{2} \\ 0.954 & \text{if } \sigma_n \leq \frac{|l|}{4} \end{cases}$$

- Similarly, probability of an edge to have a wrong oriented edge normal.

$$P\{\tilde{\mathbf{n}}_l \in \Omega_2\} = \begin{cases} 0.318 & \text{if } \sigma_n \leq \frac{|l|}{2} \\ 0.046 & \text{if } \sigma_n \leq \frac{|l|}{4} \end{cases}$$

Due to the presence of a noise, if a vertex dislocation is bigger than half of the edge size then edge flipping may occur. We can state it similar to the sampling theorem, where a signal can be reconstructed properly if and only if the data is sampled with a frequency bigger that twice the highest frequency of the data signal. Similarly, we can model the uniformly distributed noise where the random variable X_n follows the uniform distribution so we can write: $\{P\{|X_n| \leq \sigma_n\} = 1$. If the noise intensity is less than half of the edge length in the geometry then there will be no edge flip as shown in the figure 17.



(a) Noise in random direction (b) Noise in normal direction

Figure 15: (a): The Cube model corrupted with Gaussian noise ($\sigma_n = 0.4l_e$) in random direction and smooth model obtained by the proposed method. (b): Same noise added in the surface normal direction only and the corresponding result. The second row shows the corresponding face normals before the face normal processing and after face normal processing. the third row shows that in both cases, our method retains the sharp features.

If the noise standard deviation is less than the half of the edge length then we can recompute the face normal with minimum artifacts.

Using the given analysis, we can give an upper bound to the standard deviation of any noise to have a minimum edge flip if the PDF(probability density function) of the noise is given. If a surface is affected by noise only in normal direction then there is no edge flip otherwise the risks will be greater. Figure 15 shows that the smooth geometry has

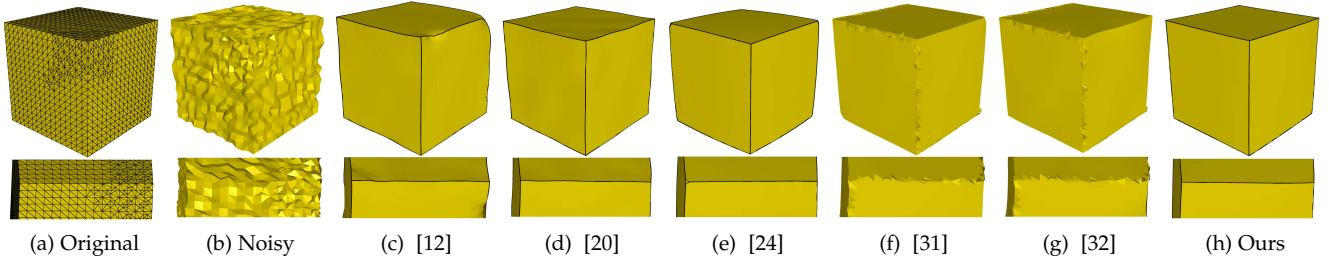


Figure 9: The Cube model consists of non-uniform triangles corrupted by Gaussian noise ($\sigma_n = 0.3l_e$) in normal direction. The first row shows the results produced by the current state of art methods and proposed method. The second row shows magnified view of one of the sharp edges in the cube model. Results show that the proposed method has sharper and straighter edges compared to the current state of art methods.

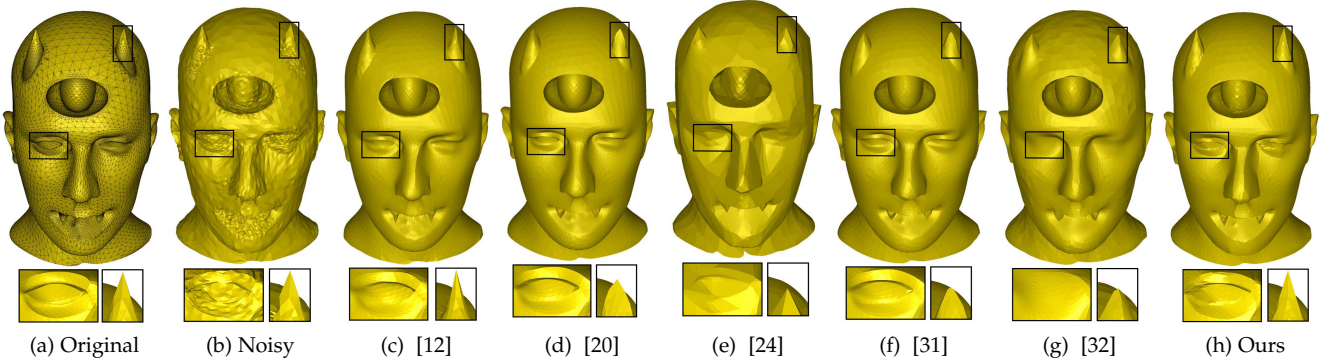


Figure 10: Devil model consists of non-uniform triangles corrupted by Gaussian noise with standard deviation $\sigma_n = 0.15l_e$. The first row shows the results produced by the current state of art methods and proposed method. The second row shows magnified view of left eye and right horn of the devil. Results show that the proposed method has minimum shrinkage at the horn area.

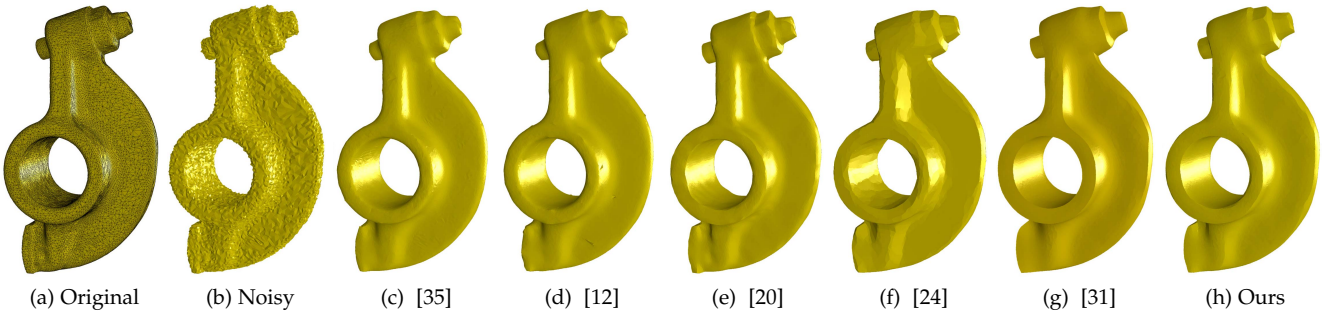


Figure 11: Rockerarm model corrupted by Gaussian noise ($\sigma_n = 0.3l_e$) in normal direction. The results are produced by the current state of art methods and proposed method.

flipped edges (red color) if the noise is added in random direction. The second row of the figure shows the wrong orientation of face normals regarding the flipped edges.

5 EXPERIMENTS, RESULTS AND DISCUSSION

We have experimented our algorithm on various kinds of CAD (figure 9, 10, 13, 12, 2, 11), CAGD (figure 5, 21) and real data (figure 19, 20, 22) models with different types of features. Our experimentation includes both synthetic and real data. Noisy surfaces with non-uniform mesh corrupted with different kinds of noise (Gaussian, Impulsive, Uniform)

are also included in our experimentation. We compared our method to several state of art denoising methods in which we implemented [35], [12], [20] and [24] based on their published article and several results of [31], [32] and [33] are provided by their authors.

Parameters: In the proposed method, we discussed about the several parameters (geometric neighbor radius r , dihedral angle threshold ρ , eigenvalue threshold τ , damping factor d and iteration p). But through out the whole experimentation, we fixed $\rho = 0.8$, $d = 3$. Effectively, we have only **3 parameters** to tune for our algorithm, in

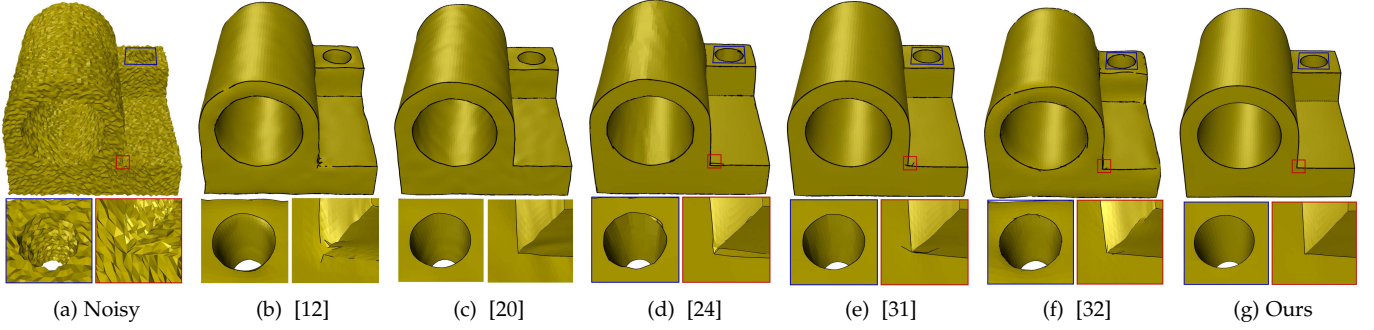


Figure 12: Non-uniform triangulated mesh surface corrupted by Gaussian noise ($\sigma_n = 0.35l_e$) in normal direction where l_e is the average edge length. The first row shows the results obtained by state of art methods and the proposed method. The second row shows the magnified view of corner and cylindrical hole of the corresponding geometry. The black curve shows the edge information in the smooth geometry and it is detected using the dihedral angle.

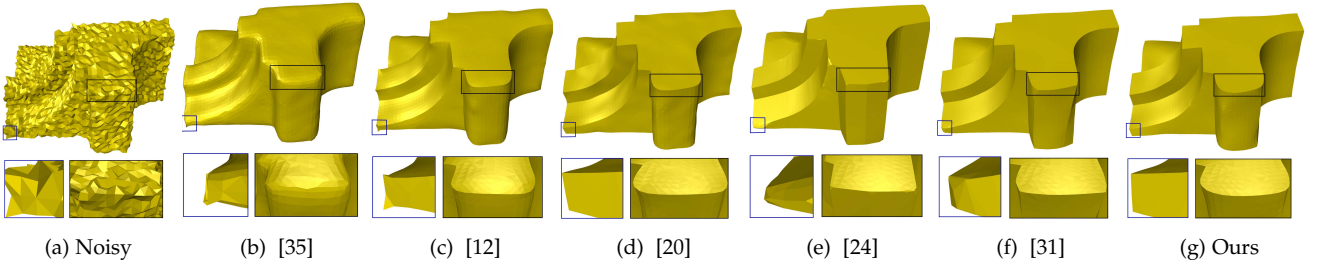


Figure 13: Fandisk model corrupted with a Gaussian noise ($\sigma_e = 0.3l_e$) in random direction. The first row shows the results produced by the current state of art methods and proposed method. The second row shows corner and cylindrical region of the concerned model. The proposed method does not produce any false feature in the umbilical region while retains the sharp features and corners.

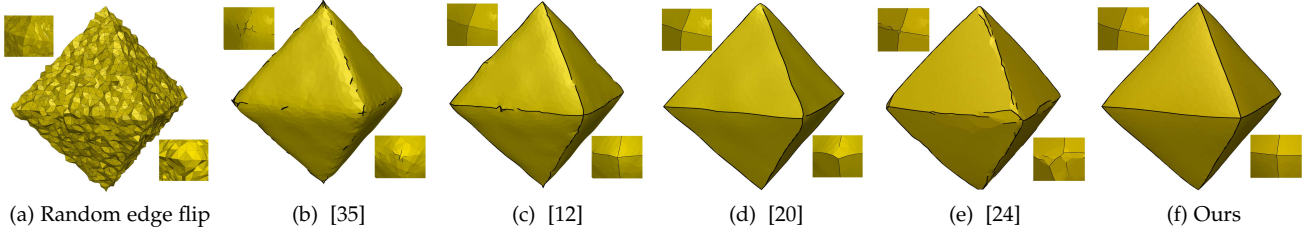


Figure 14: Robustness against random edge flips after adding noise. (a): Noisy model corrupted with $\sigma_n = 0.3l_e$ and random edge flips, (b) to (f) show corresponding results with state of art methods and the proposed method.

which τ is the most important which depends on intensity of noise but at the same time this parameter is not highly sensitive. We use $\tau = (0.3 - 0.4)$ for synthetic data and $\tau = (0.05 - 0.1)$ for real data because real data have smaller noise intensity compared to synthetic data in our experiments. The neighborhood radius r depends on the average edge length of the geometry. We iterate several times ($p = 40 - 60$) to have a better result using the proposed method. In the quantitative comparison table, the parameters are given in the following format: (τ, r, p) . For the [31] and [32] methods, we mention *Default* in the parameter column because smooth models are provided by those authors. We are following a similar pattern for other algorithms too. (σ_c, σ_s, p) for [35], (σ_s, p) for [20], (λ, s, p)

for [12] and (α) for [24], where σ_s, σ_c are the standard deviation of the Gaussian function in the bilateral weighting. s and λ represent the step size and the smoothing threshold. The term α controls the amount of smoothing.

Visual Comparison: We tested on models corrupted with Gaussian, Impulsive and Uniform noise in random and surface normal direction. The Joint (figure 12), Devil (figure 10), Cube (figure 9) and Block (figure 2) have non-uniform meshes corrupted with Gaussian noise in random direction. Figure 12 shows that the proposed method produces a smooth model with sharp features without creating any false features (piecewise flat area like [24]) while the method [20] does not manage to remove the low frequency noise (we can see as smooth ripples). The method [31] produces

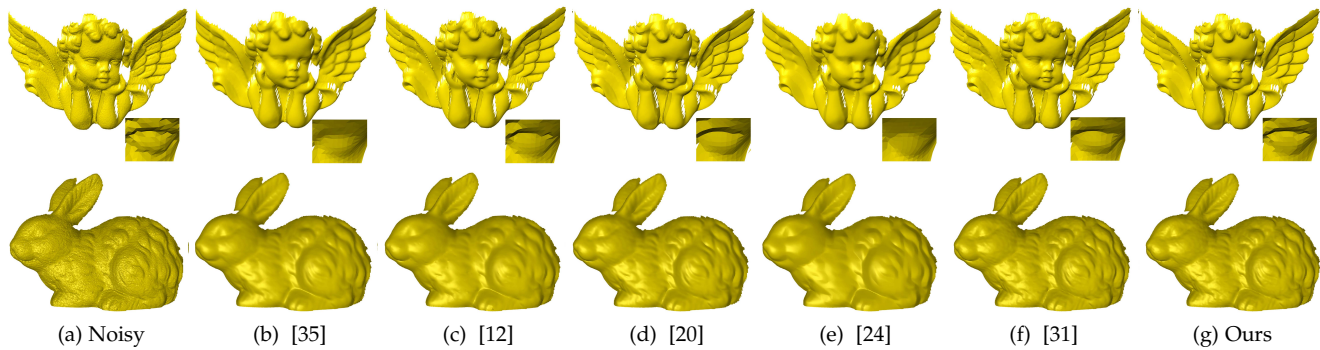


Figure 19: Triangulated mesh surface (**real data**) corrupted by 3D scanner noise. Both rows show the results obtained by state of art methods and proposed method for Angel and Rabbit models.

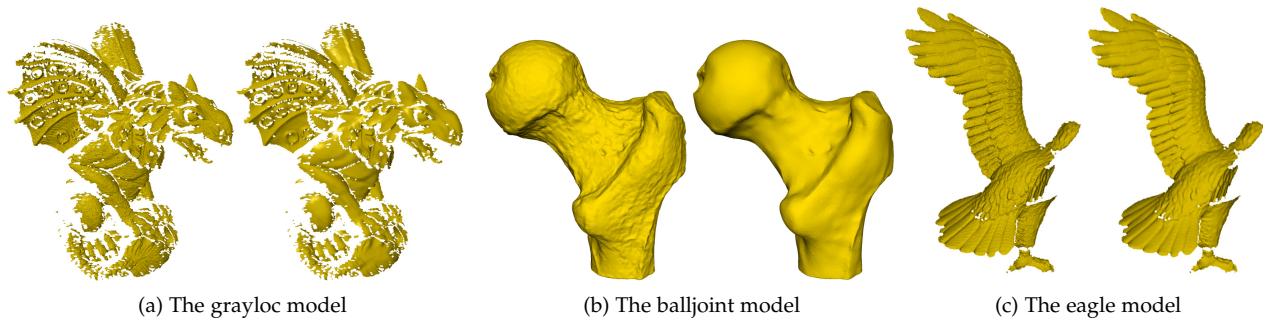


Figure 20: Results obtained by our method against different kinds of real data captured by the laser scanner. The figure a and c show real life scans with a lot of holes and our method manage to produce good results.

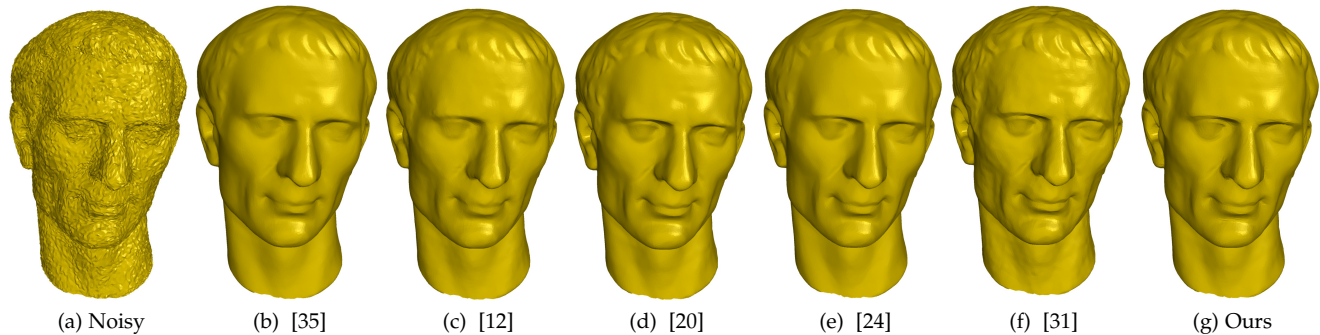


Figure 21: The Julius model corrupted by Gaussian noise ($\sigma_n = 0.2l_e$) in random direction. The results are produced by the current state of art methods and proposed method. Our method does not outperform compared to the current state art method and produces quite similar to the [20] method. The proposed method removes low frequency noise also better than the method [31] where we can see small ripples of noise on the Julius model.

good results but at the narrow cylindrical area it could not manage to retain the circular area. It also produces some false features at the non-uniform sharp corner. The [32] method could not manage to retain the sharp features. Similarly, we can see this behavior for the Cube model in figure 9. Figure 10 shows the robustness of the proposed method against volume shrinkage. The horns of the model have the minimum shrinkage with the proposed method compared to the state of art methods. The Rockerarm model (figure 11) has a considerably non-uniform mesh and our method better retains sharp features (the screw part) com-

pared to [31], [12], [35] while removing the noise better compared to the methods [20] [24]. The Fandisk model contains of both cylindrical and sharp feature regions. In our experimentation, this model is corrupted by high intensity Gaussian noise in random direction and figure 13 shows that the proposed method delivers both sharp features and umbilical regions without noise component and false features. Our method is invariant against different kinds of noise as shown in figure 17 where the vase model is corrupted by impulsive and uniform noise. The proposed method does not produce appropriate results above a certain level

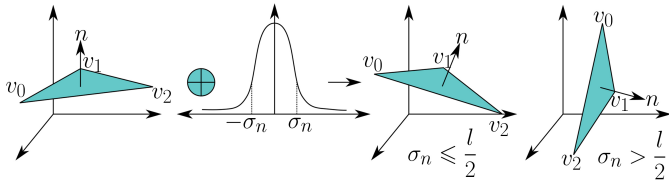


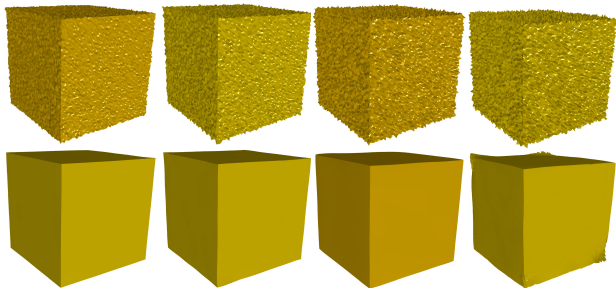
Figure 16: Noise and edge length analysis in \mathcal{R}^3 (left to right): A triangle without noise, then we add Gaussian noise with standard deviation σ_n . For small σ_n the normal of the noisy mesh has most likely positive scalar product with the correct normal. For big σ_n , normals can have wrong orientation.



(a) Original (b) Impulse (c) Ours (d) Uniform (e) Ours

Figure 17: Results obtained by our method against different kinds of noise. (a): Original vase model, (b): 1/3 of the vertices of the vase model are corrupted by impulsive random noise, (c): Corresponding result with our method, (d): the vase model is corrupted by uniformly distributed noise and (e): corresponding result.

of noise as shown in figure 18. Figure 14 shows that our method is robust against random edge flips. We compared our algorithm with real data as shown in figures 19 and 22. For the real data, we can not see considerable differences between the proposed method and state of art denoising methods because the noise intensity is quite low and state



(a) $\sigma_n = 0.4l_e$ (b) $\sigma_n = 0.6l_e$ (c) $\sigma_n = 0.8l_e$ (d) $\sigma_n = l_e$

Figure 18: Robustness against different level of noise: The first row shows the cube model corrupted with different level of noise. The second row shows the corresponding results obtained by the proposed method. In figure (d), noise level is bigger than feature size and it is impossible to decouple features from noise. As a result, we are not able to recover the perfect cube.

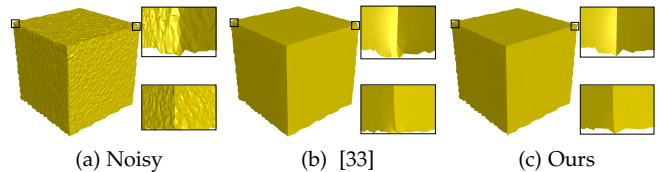


Figure 22: Scanned cube model (**real data**) and results obtained using [33] and the proposed method.

of art methods also produce good results. Figure 19 shows that our method better retains features in the right eye of the angel model. Similarly, figure 22 shows that our method better retains sharp features at the corners compared to [33]. Figure 20 shows the robustness of the proposed algorithm against irregular meshes and holes in the real data. The Greyloc and the Eagle model has a lot holes and spikes but our smoothing algorithm manages to produce the smooth surface along with proper features.

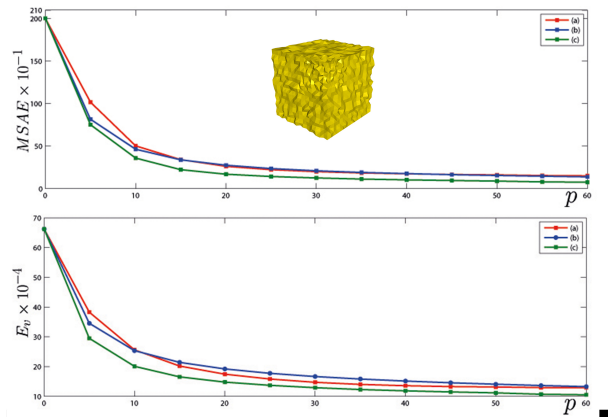


Figure 23: Convergence plot comparison between (a): [12], b: [20] and (c): our method. The error metrics MSAE and E_v are computed for the Cube model and p is the number of iterations.

Quantitative Comparison: In this section, we give a quantitative comparison of our method with the current state of art methods. We are using two different parameters: E_v (L^2 vertex-based error) and MSAE (the mean square angular error) used in current state of art methods. E_v computes the positional error from the original ground truth model and is defined as [22]:

$$E_v = \sqrt{\frac{1}{3 \sum_{k \in F} \sum_{i \in V} \sum_{j \in F_v(i)} A_j \text{dist}(\tilde{v}_i, T)^2}}$$

Where F is the triangular element set and V represents the set of vertices. A_k and A_j show corresponding element area and $F_v(i)$ shows the number of elements in the i^{th} vertex-ring. $\text{dist}(\tilde{v}_i, T)$ is the closest L_2 distance between the newly computed vertex \tilde{v}_i and the triangle T of the reference model.

The MSAE computes the orientation error between the original model and the smooth model and defined as :

$$MSAE = E[\angle(\tilde{\mathbf{n}}, \mathbf{n})]$$

Where $\tilde{\mathbf{n}}$ is the newly computed face normal and \mathbf{n} represents the face normal of the reference model. E stands for the expectation value. The quantitative comparison table shows that our method performs better for most of the models e.g. Cube, Devil, Joint etc. For some model like Fandisk, our method produces quite similar numeric errors as state of art methods.

Convergence: Our smoothing algorithm guarantees convergence because of the eigenvalue binary optimization. Modification of the eigenvalues of the tensor will not affect the orientation of the corresponding face normal when noise is removed because the difference between two eigenvalues will be zero and also the less dominant eigenvalue will be zero. There will be no more modification on noisy surfaces after some iteration when we met the explained scenario as shown in figure 8, where there is no significant change (visually) after 60 iterations. Figure 23 shows that the proposed method converges with minimum error compared to the [12] and [20] methods. We can see that after 40 iterations, our method is almost stable and does not produce significant changes. The eigenvalues binary optimization not only helps in preserving features but also improves the convergence rate of the algorithm.

Running Complexity: Our implementation is quite straight forward. The neighborhood computation is done by the growing disk method to compute the element based normal voting tensor. The tensor computation has the complexity of $O(c \cdot n_f \cdot p)$, where c is the number of elements within the neighborhood, n_f and p are the number of elements and iterations. The tensor multiplication procedure has the running complexity of $O(n_f)$. Similarly, the vertex update procedure has the complexity of $O(c \cdot n_v \cdot p)$, where n_v is the number of vertices in the geometry. In general, $n_f > n_v$, so overall complexity of the algorithm will be $O(c \cdot n_f \cdot p)$.

6 CONCLUSION AND FUTURE WORK

In this paper, we presented a simple and effective tensor multiplication algorithm for feature preserving mesh denoising. The concept of element based normal voting tensor has been introduced and eigenanalysis of this tensor leads to decoupling the features from noise. We have shown that the proposed method does not need any additional Laplacian based smoothing technique required to remove the noise like multistage state of arts methods [27] [28] [31] [32]. Our method removes noise by multiplying the element based NVT to the corresponding face normal, and that reduces the complexity of the algorithm. We have introduced the concept of eigenvalue binary optimization that not only enhances sharp features but also improves the convergence rate of the proposed algorithm. The local binary neighborhood selection helps to select the similar elements in the neighborhood to compute the element based normal voting tensor which avoids feature blurring during the denoising process. We provide a stochastic analysis of the noise effect on the geometry depending on the average edge length of the triangulated mesh. On the basis of this analysis, we can provide an upper bound to the noise standard deviation depending on the average edge length to reconstruct the smooth surface from the noisy surface. The experimentation results (visual and quantitative) show the capability of the proposed algorithm. Our method produces good results not only in terms of visual but also quantitatively with all kind of data including CAD, CAGD and real data. We have also shown the robustness of the algorithm against different kinds and levels of noise. Our algorithm performs well against different kinds of noise. We discussed the wrong orientation of triangles in presence of strong noise. In future work, we would like to solve this problem of edge flips. We plan to extend our algorithm not only for point set smoothing but also to smooth any vector field in \mathbb{R}^3 space.

APPENDIX A

RELATION BETWEEN THE SHAPE OPERATOR AND THE ELEMENT BASED NVT

Let us consider a smooth manifold surface \mathcal{M} embedded in \mathbb{R}^3 . We assume that the surface is orientable and it has well defined normal $N : \mathcal{M} \rightarrow S^2$ on \mathcal{M} . Then we can define our proposed tensor $C_\Omega : \mathbb{R}^3 \rightarrow \mathbb{R}$:

$$C_\Omega = \int_\Omega (n \cdot n^T) d\Omega$$

Where $n \in N$ and Ω is local neighborhood area of point p . The neighborhood area is shown in figure 24 (A).

To compute the shape operator on a surface, the surface must be C^2 and properly oriented. The shape operator is defined on the tangent plane $\mathcal{S} : T_p\mathcal{M} \times T_p\mathcal{M} \rightarrow \mathbb{R}$. $T_p\mathcal{M}$ represents the tangent plane, spanned by the basis vectors ξ_1 and ξ_2 . The eigenvalues of the shape operator \mathcal{S} are the principle curvatures κ_1 and κ_2 and eigenvectors will be the basis of the tangent plane (ξ_1, ξ_2) . The eigenvectors are termed as the principle curvature directions.

Represented in the orthonormal basis of the normal and the principle curvature directions, the surface normal in a local neighborhood of point p can be approximated by:

$$n(\xi_i, \xi_2) = [1, \kappa_1 \xi_1, \kappa_2 \xi_2]$$

Quantitative Comparison				
Models	Methods	MSE	$E_v (\times 10^{-3})$	Parameters
Cube $ F = 3808$ $ V = 1906$	[35]	5.267	3.142	(0.3,0.3,30)
	[12]	1.935	1.432	(0.05,0.05,50)
	[20]	1.159	1.207	(0.3,60)
	[24]	1.343	4.476	(1.4)
	[31]	40.41	1.166	(Default)
	[32]	41.63	1.446	(Default)
Ours	0.700	1.034	(0.3,0.1,50)	
Devil $ F = 25906$ $ V = 12986$	[35]	4.983	58.86	(0.3,0.3,20)
	[12]	3.444	32.53	(0.2,0.05,30)
	[20]	2.641	8.95	(0.3,50)
	[24]	6.699	26.28	(4.0)
	[31]	2.870	9.44	(Default)
	[32]	5.396	13.52	(Default)
Ours	2.702	6.901	(0.1, 1.0,30)	
Joint $ F = 52226$ $ V = 26111$	[35]	3.777	0.530	(0.3,0.3, 40)
	[12]	2.630	0.766	(0.009,0.05,50)
	[20]	1.808	0.263	(0.4, 100)
	[24]	1.768	0.500	(1.4)
	[31]	0.956	0.179	(Default)
	[32]	2.874	0.366	(Default)
Ours	0.829	0.171	(0.3, 0.05, 60)	
Fandisk $ F = 12946$ $ V = 6475$	[35]	8.567	4.422	(0.4,0.4,40)
	[12]	5.856	4.910	(0.07,0.05,30)
	[20]	2.727	1.877	(0.4,70)
	[24]	4.788	5.415	(1.4)
	[31]	2.221	1.702	(Default)
	[32]	2.692	1.964	(0.3, 0.2, 60)
Ours	5.737	44.22	(0.3,0.3,40)	
Rockerarm $ F = 48212$ $ V = 24106$	[12]	5.982	51.35	(0.2,0.05,50)
	[20]	5.713	23.47	(1.0, 100)
	[24]	7.468	34.70	(1.4)
	[31]	6.846	30.45	(Default)
	[32]	5.410	20.05	(0.3,1.0,60)
	Ours	5.410	20.05	(0.3,1.0,60)

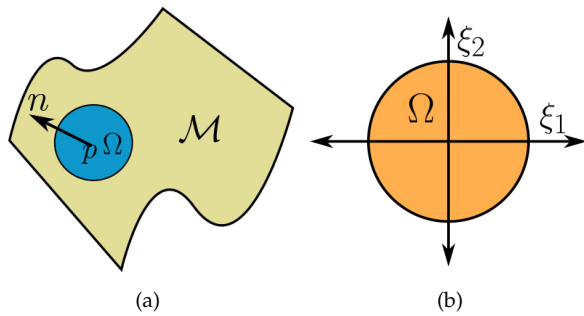


Figure 24: Smooth manifold surface \mathcal{M} with proper oriented normal.

Now, we can compute the covariance matrix using the above normal vector:

$$n^T \cdot n = \begin{bmatrix} 1 & \kappa_1 \xi_1 & \kappa_2 \xi_2 \\ \kappa_1 \xi_1 & \kappa_1^2 \xi_1^2 & \kappa_1 \xi_1 \kappa_2 \xi_2 \\ \kappa_2 \xi_2 & \kappa_1 \xi_1 \kappa_2 \xi_2 & \kappa_2^2 \xi_2^2 \end{bmatrix} \quad (7)$$

For a small symmetric Ω as shown in figure 24 (B), the integral for the off-diagonal components will be zero:

$$\int_{\Omega} n^T \cdot n d\Omega = \begin{bmatrix} 1 & 0 & 0 \\ 0 & \kappa_1^2 \xi_1^2 & 0 \\ 0 & 0 & \kappa_2^2 \xi_2^2 \end{bmatrix} \quad (8)$$

So by this approximation, the shape operator is contained in the covariance matrix as the lower right 2×2 sub-matrix. Therefore the second and third eigenvalue of the NVT approximate the squares of the principal curvatures κ_1 and κ_2 .

REFERENCES

- [1] M. Botsch, M. Pauly, C. Ross, S. Bischoff, and L. Kobbelt, "Geometric modeling based on triangle meshes," in *ACM SIGGRAPH 2006 Courses*, ser. SIGGRAPH '06. New York, NY, USA: ACM, 2006.
- [2] M. Botsch, P. Alliez, L. Kobbelt, M. Pauly, and B. Lévy, *Polygon mesh processing*. Natick, Mass. A K Peters, 2010.
- [3] D. A. Field, "Laplacian smoothing and delaunay triangulations," *Communications in Applied Numerical Methods*, vol. 4, no. 6, pp. 709–712, 1988.
- [4] M. Desbrun, M. Meyer, P. Schröder, and A. H. Barr, "Implicit fairing of irregular meshes using diffusion and curvature flow," in *Proceedings of the 26th Annual Conference on Computer Graphics and Interactive Techniques*, ser. SIGGRAPH '99. New York, NY, USA: ACM Press/Addison-Wesley Publishing Co., 1999, pp. 317–324.
- [5] M. Alexa, "Differential coordinates for local mesh morphing and deformation," *The Visual Computer*, vol. 19, no. 2-3, pp. 105–114, 2003.
- [6] Z.-X. Su, H. Wang, and J.-J. Cao, "Mesh denoising based on differential coordinates," in *Shape Modeling and Applications, 2009. SMI 2009. IEEE International Conference on*, June 2009, pp. 1–6.
- [7] O. Sorkine, "Differential representations for mesh processing," *Computer Graphics Forum*, vol. 25, no. 4, pp. 789–807, 2006.
- [8] P. Perona and J. Malik, "Scale-space and edge detection using anisotropic diffusion," *Pattern Analysis and Machine Intelligence, IEEE Transactions on*, vol. 12, no. 7, pp. 629–639, Jul 1990.
- [9] U. Clarenz, U. Diewald, and M. Rumpf, "Anisotropic geometric diffusion in surface processing," in *Proceedings of the Conference on Visualization '00*, ser. VIS '00. Los Alamitos, CA, USA: IEEE Computer Society Press, 2000, pp. 397–405.
- [10] C. L. Bajaj and G. Xu, "Anisotropic diffusion of surfaces and functions on surfaces," *ACM Trans. Graph.*, vol. 22, no. 1, pp. 4–32, Jan. 2003.
- [11] T. Tasdizen, R. Whitaker, P. Burchard, and S. Osher, "Geometric surface smoothing via anisotropic diffusion of normals," in *Proceedings of the Conference on Visualization '02*, ser. VIS '02. Washington, DC, USA: IEEE Computer Society, 2002, pp. 125–132.
- [12] K. Hildebrandt and K. Polthier, "Anisotropic filtering of non-linear surface features," *Computer Graphics Forum*, vol. 23, pp. 391–400, 2004.
- [13] D. Barash, "Fundamental relationship between bilateral filtering, adaptive smoothing, and the nonlinear diffusion equation," *Pattern Analysis and Machine Intelligence, IEEE Transactions on*, vol. 24, no. 6, pp. 844–847, Jun 2002.
- [14] C. Tomasi and R. Manduchi, "Bilateral filtering for gray and color images," in *Proceedings of the Sixth International Conference on Computer Vision*, ser. ICCV '98. Washington, DC, USA: IEEE Computer Society, 1998, pp. 839–846.
- [15] J. Solomon, K. Crane, A. Butscher, and C. Wojtan, "A general framework for bilateral and mean shift filtering," *ArXiv e-prints*, vol. 32, April 2014.
- [16] G. Taubin, "Linear anisotropic mesh filtering," in *IBM Research Report RC22213(W0110-051)*, IBM T.J. Watson Research, 2001.
- [17] H. Yagou, Y. Ohtake, and A. Belyaev, "Mesh smoothing via mean and median filtering applied to face normals," in *Geometric Modeling and Processing, 2002. Proceedings, 2002*, pp. 124–131.
- [18] Y. Ohtake, A. Belyaev, and H. Seidel, "Mesh smoothing by adaptive and anisotropic gaussian filter applied to mesh normals," in *IN VISION MODELING AND VISUALIZATION, 2002*.
- [19] H. Yagou, Y. Ohtake, and A. Belyaev, "Mesh denoising via iterative alpha-trimming and nonlinear diffusion of normals with automatic thresholding," in *Computer Graphics International, 2003. Proceedings, July 2003*, pp. 28–33.
- [20] Y. Zheng, H. Fu, O.-C. Au, and C.-L. Tai, "Bilateral normal filtering for mesh denoising," *Visualization and Computer Graphics, IEEE Transactions on*, vol. 17, no. 10, pp. 1521–1530, Oct 2011.
- [21] H. Zhang, C. Wu, J. Zhang, and J. Deng, "Variational mesh denoising using total variation and piecewise constant function space," *IEEE Transactions on Visualization and Computer Graphics*, vol. 21, no. 7, pp. 873–886, July 2015.
- [22] X. Sun, P. Rosin, R. Martin, and F. Langbein, "Fast and effective feature-preserving mesh denoising," *Visualization and Computer Graphics, IEEE Transactions on*, vol. 13, no. 5, pp. 925–938, Sept 2007.
- [23] L. Xu, R. Wang, J. Zhang, Z. Yang, J. Deng, F. Chen, and L. Liu, "Survey on sparsity in geometric modeling and processing," *Graphical Models*, vol. 82, pp. 160 – 180, 2015.
- [24] L. He and S. Schaefer, "Mesh denoising via l0 minimization," *ACM Trans. Graph.*, vol. 32, no. 4, pp. 64:1–64:8, Jul. 2013.
- [25] R. Wang, Z. Yang, L. Liu, J. Deng, and F. Chen, "Decoupling noise and features via weighted l1-analysis compressed sensing," *ACM Trans. Graph.*, vol. 33, no. 2, pp. 18:1–18:12, Apr. 2014.
- [26] X. Wu, J. Zheng, Y. Cai, and C.-W. Fu, "Mesh Denoising using Extended ROF Model with L1 Fidelity," *Computer Graphics Forum*, 2015.
- [27] H. Fan, Y. Yu, and Q. Peng, "Robust feature-preserving mesh denoising based on consistent subneighborhoods," *IEEE Transactions on Visualization and Computer Graphics*, vol. 16, no. 2, pp. 312–324, Mar. 2010.
- [28] Z. Bian and R. Tong, "Feature-preserving mesh denoising based on vertices classification," *Comput. Aided Geom. Des.*, vol. 28, no. 1, pp. 50–64, Jan. 2011.
- [29] H. S. Kim, H. K. Choi, and K. H. Lee, "Feature detection of triangular meshes based on tensor voting theory," *Computer-Aided Design*, vol. 41, no. 1, pp. 47 – 58, 2009.
- [30] G. Medioni, "Tensor voting: Theory and applications," 2000.
- [31] W. Zhang, B. Deng, J. Zhang, S. Bouaziz, and L. Liu, "Guided mesh normal filtering," *Computer Graphics Forum (Special Issue of Pacific Graphics 2015)*, vol. 34, pp. 23–34, 2015.
- [32] M. Wei, J. Yu, W. M. Pang, J. Wang, J. Qin, L. Liu, and P. A. Heng, "Bi-normal filtering for mesh denoising," *IEEE Transactions on Visualization and Computer Graphics*, vol. 21, no. 1, pp. 43–55, Jan 2015.
- [33] X. Lu, Z. Deng, and W. Chen, "A robust scheme for feature-preserving mesh denoising," *IEEE Transactions on Visualization and Computer Graphics*, vol. 22, no. 3, pp. 1181–1194, March 2016.
- [34] T. Ojala, M. Pietikainen, and D. Harwood, "A comparative study of texture measures with classification based on featured distributions," *Pattern Recognition*, vol. 29, no. 1, pp. 51–59, Jan. 1996.

- [35] S. Fleishman, I. Drori, and D. Cohen-Or, "Bilateral mesh denoising," in *ACM SIGGRAPH 2003 Papers*, ser. SIGGRAPH '03. New York, NY, USA: ACM, 2003, pp. 950–953.
- [36] X. Sun, P. Rosin, R. Martin, and F. Langbein, "Noise in 3d laser range scanner data," in *Shape Modeling and Applications, 2008. SMI 2008. IEEE International Conference on*, June 2008, pp. 37–45.